Electronic Supplementary Material (ESI) for Physical Chemistry Chemical Physics.

Supporting Information for

Dynamic Effects of Spine of Hydrated Magnesium on Viral RNA Pseudoknot Structure

Vysakh Ramachandran[†], Avijit Mainan[†] and Susmita Roy*[†]

[†] Department of Chemical Sciences, Indian Institute of Science Education and Research Kolkata, West Bengal 741246

This PDF file includes:
Supporting Information:

- Method details
  - Force field and parameters used in explicit solvent simulations
  - Potential terms of DCC model
  - Table S1 showing DCC parameters
  -
- Supporting Results:
  - Visiting Frequency
- Supporting Figures:
  - Figures S1 to S17
- References for Supporting Information:

1. Force field modifications to accommodate first Residue GTP

In Beet western yellow virus (BWYV) RNA Pseudoknot (PK) structure 437D [1], GTP is the first residue, but Amber 99 force field [2] with modifications parmbsc051 [3] and chiOL3 [4] cannot accommodate first residue GTP as part of RNA PK. Hence, we modified the rna.n (terminal database) file in the force field to remove hydrogen at the 5' terminal of second residue of RNA PK then GTP is connected with it by bonds and we make sure all local and non-local interactions between first and second residue junction ((O3' of GTP1 and P of G2) were similar as to the other junctions.

1.1 Parameters of explicit solvent simulation

All explicit solvent simulation were performed using the Amber 99 force field [2] with parmbsc051 [3] and chiOL3 [4] extensions to generate the topology. For K^+, modified K^+ parameters [7] were used to avoid the crystallization in higher concentration limit, and for Mg^{2+} , newly derived parameters of Mg^{2+} by Villa and co-workers were used with Tip3p water model [8] as it is shown to reproduce experimental kinetic data of binding for water and Mg^{2+} ions. However, further improvement is required for Mg^{2+}-Phosphate interaction. It is important to note here that there are ongoing research efforts towards curating, comparing, and developing accurate Mg^{2+} force fields[9,10].

2. Description of additional terms in the DCC model potential

The mixing free energy within the effective Gaussian shell volume is given as,

$$V_{Mix} = \sum_i \sum_k k_B T n_{Mix,ik} \tau_{eff,i} \ln\left(\frac{n_{Mix,ik}}{ec_k}\right). \quad \text{(S1)}$$

Where e is the Euler's number. $n_{Mix,ik}$ is the mixing charge density, which is allotted with Gaussian mixing charges and screening charges,

$$n_{Mix,ik} = c_k\left(1 - \frac{z_k \phi_\mu\left(\vec{r_i}\right)}{k_B T}\right) + n_{\mu,k}\left(\vec{r_i}\right) \quad \text{(S2)}$$

Two other Harmonic potentials, V_{Hole} and V_{Rest} are added to restrain the charges within their restricted volume region and are given respectively [5],

$$V_{Hole,ik} = \frac{1}{2} k_{Hole} \sum_i \sum_k n^2_{Hole,ik} \quad \text{(S3)}$$

where,

$$n_{Hole,ik} = c_k\left(1 - \frac{z_k \phi_\mu\left(\vec{r_i}\right)}{k_B T}\right) + n_{\mu,k}\left(\vec{r_i}\right) + n_{\eta,k}\left(\vec{r_i}\right). \quad \text{(S4)}$$

and

$$V_{Rest} = \frac{1}{2} k_w \sum_i \sum_k \left(\mu_{i,k} - n_{\mu,k}\left(\vec{r_i}\right)\tau_{\mu,i}\right)^2 + \frac{1}{2} k_w \sum_i \sum_k \left(\eta_{i,k} - n_{\eta,k}\left(\vec{r_i}\right)\tau_{\eta,i}\right)^2. \quad \text{(S5)}$$

3 . The parameter set we used in current simulation is given in Table S1.

Reduced parameter set	
τ_R	2ps
μ_R	15amu
ε_R	3.75 KJ/mol
T_R	3.75K
SBM Potential parameter	
k_r	$2 \times 10^4\ \varepsilon_R / nm^2$
k_θ	$40\ \varepsilon_R / rad^2$
k_χ	$10\ \varepsilon_R / rad^2$
k_{NC}	$1.33\ k_B T$
$k_{innerMg-RNA}$	$5.69\ k_B T$
Excluded volume parameter	
σ_{NC}	0.17 nm
$\sigma_{innerMg-RNA}$	0.19 nm
$\sigma_{outerMg-RNA}$	0.34 nm
σ_{Mg-Mg}	0.56 nm
Ion condensation parameter	
σ_μ	0.7 nm
σ_η	0.34 nm (for KCl) & 0.2467 nm (for NaCl)
k_{Hole}	$10^4\ k_B T / P\left(0, \sigma_\eta^2\right)$
k_w	$1\ k_B T$

$*\sigma_{NC}$, $\sigma_{innerMg-RNA}$, $\sigma_{outerMg-RNA}$, σ_{Mg-Mg} are defined in terms of $\sigma_{contact-type}$ in the main manuscript.

4 . Visiting frequency

RNA is a negatively charged polymer and closely interacts with cations involved in mixed salt of K^+ and Mg^{2+}. Their interactions have been very selective as determined by the nature of RNA atoms and ions. Because the inner and outer sphere ions interact with RNA more closely and have a greater structural influence on it, their interactions must be investigated. Thus, it can be quantified using Visiting frequency, how frequently ions visit the atoms of RNA. The Cut off to consider it as a visit is determined by the Radial distribution function (RDF) of Ions around RNA (**Figure S3** and **Figure S6(a)**). The Visiting frequency is calculated using following equation:

$$Visiting\ frequency = \frac{\int_{o}^{T} \rho \, dt}{T}$$

Where $\rho = 1$, when an ion is within the cutoff at a specific RNA atom.

$\rho = 0$, for else

T is the total time we are observing. Cutoffs for the ions are:

(i) From RDF of K^+ ion around O and N of RNA

Inner sphere K^+ ion = 3.6 Å

Outer Sphere K^+ ion = 3.6 - 6 Å

(ii) From RDF of Mg^{2+} ion around O and N of RNA

Inner Sphere Mg^{2+} ion = 0 - 3 Å

Outer Sphere Mg^{2+} ion = 3 - 5.5 Å

(iii) From RDF of Mg^{2+} ion around P of RNA

Inner Sphere Mg^{2+} ion = 0 - 3.5 Å

Outer Sphere Mg^{2+} ion = 5.5 to 6.5 Å

Population distributions

It measures the number of particular types of ions in an ion atmosphere around the whole RNA. More specifically, we calculate the distribution of the inner sphere or outer-sphere of ions such as K^+ and Mg^{2+} around whole RNA in each frame of MD simulation.

Supporting Figures

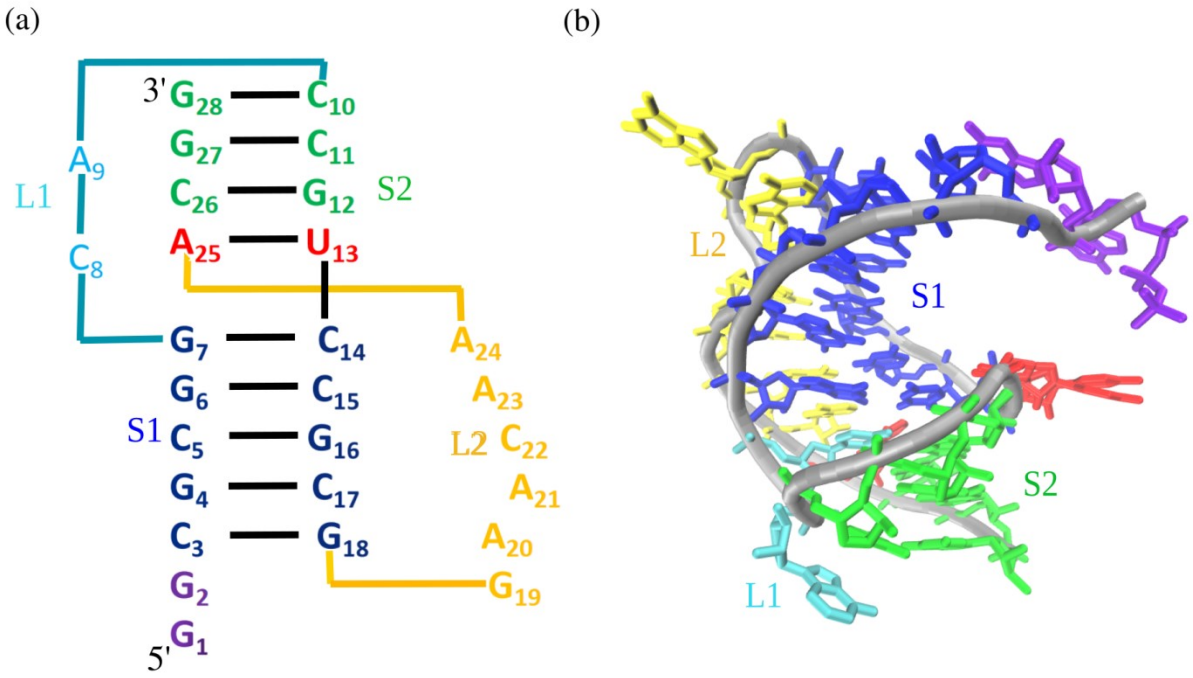

Figure S1: BWYV RNA PK Structure. (a) Secondary structure of RNA PK (b) Tertiary structure of RNA PK (Snapshot taken from PDB ID: 437D) [1]. Here Stem1 is represented by S1, Stem2 is represented by S2, Loop 1 is represented by L1, and Loop2 is represented by L2.

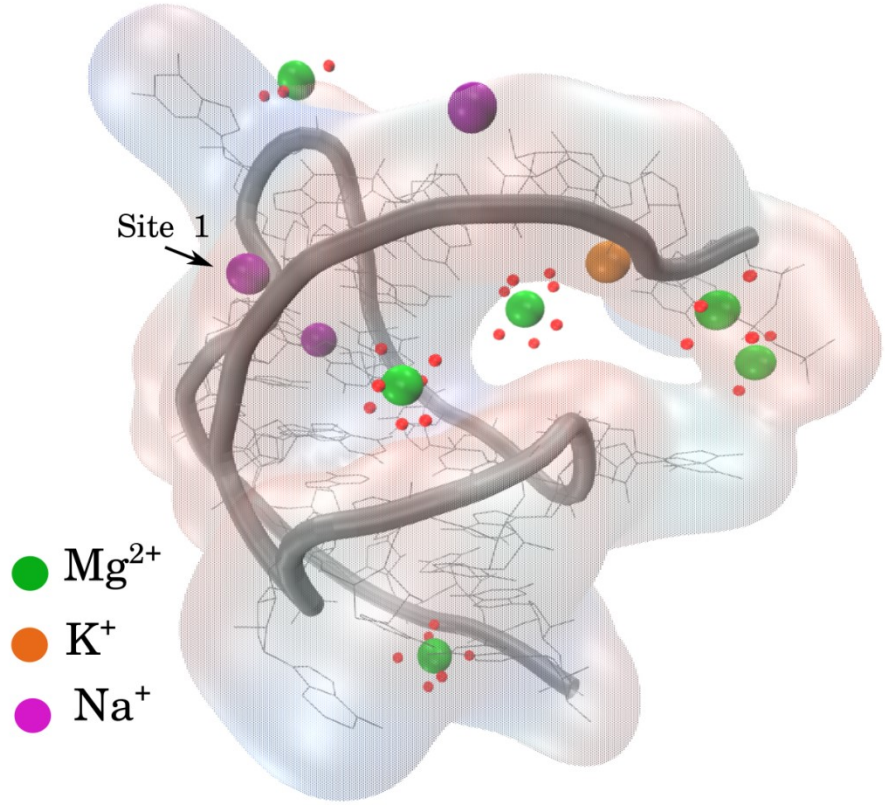

Figure S2: BWYV RNA PK with ions taken from the XRD experiment (PDB ID: 1L2X) [6].

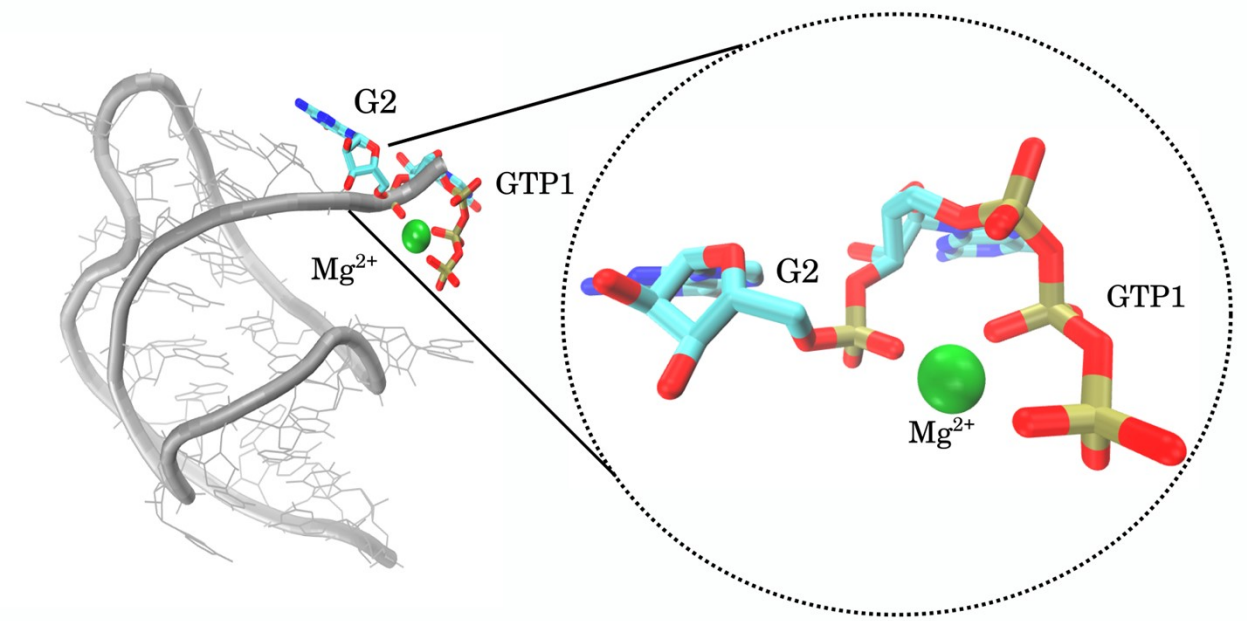

Figure S3: Mg^{2+} chelation between first residue GTP and second residue G. Left: BWYV RNA PK (437D) snapshot showing first two residues and chelated Mg^{2+}. Right: Image of how Mg^{2+} ion is connected with the first two residues.

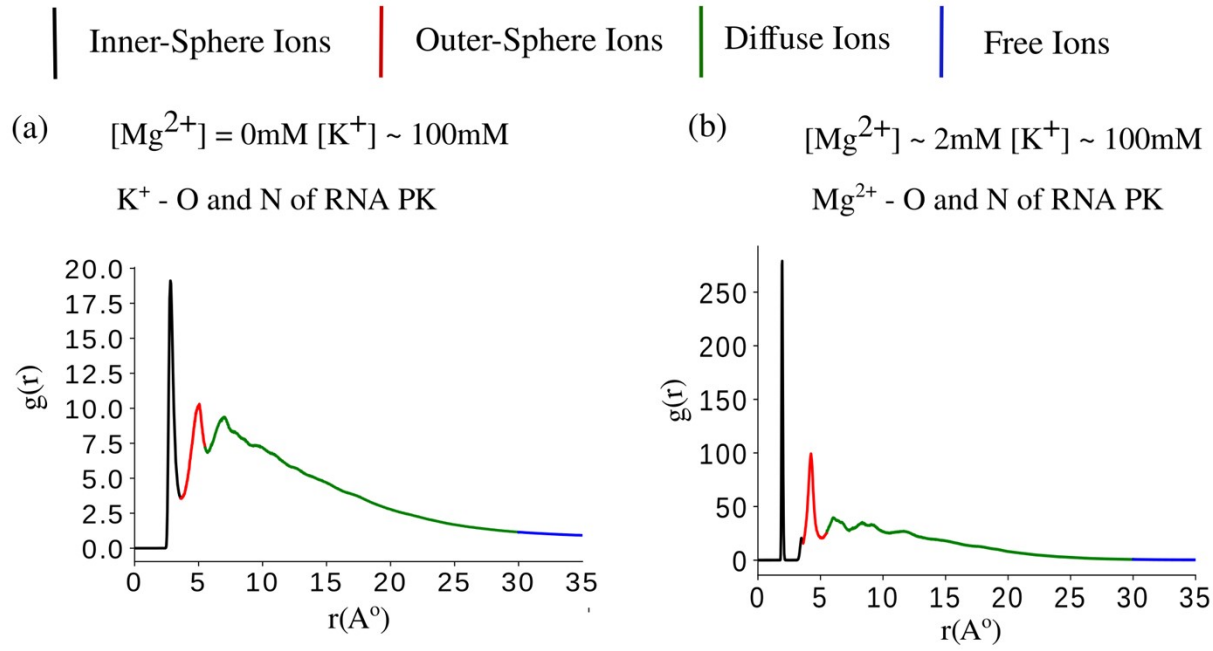

Figure S4: Classification of ions depending on the distance from RNA PK are: Inner-Sphere ions (black), Outer-Sphere ions (Red), Diffuse ions (Green) and Free Ions (Blue), Which is reflected in the radial distribution function (RDF) of (a) K^+ around the O and N of RNA PK at $[Mg^{2+}] = 0$mM and $[K^+] \sim 100$mM and (b) Mg^{2+} around the O and N of RNA PK at $[Mg^{2+}] \sim 2$mM and $[K^+] \sim 100$mM .

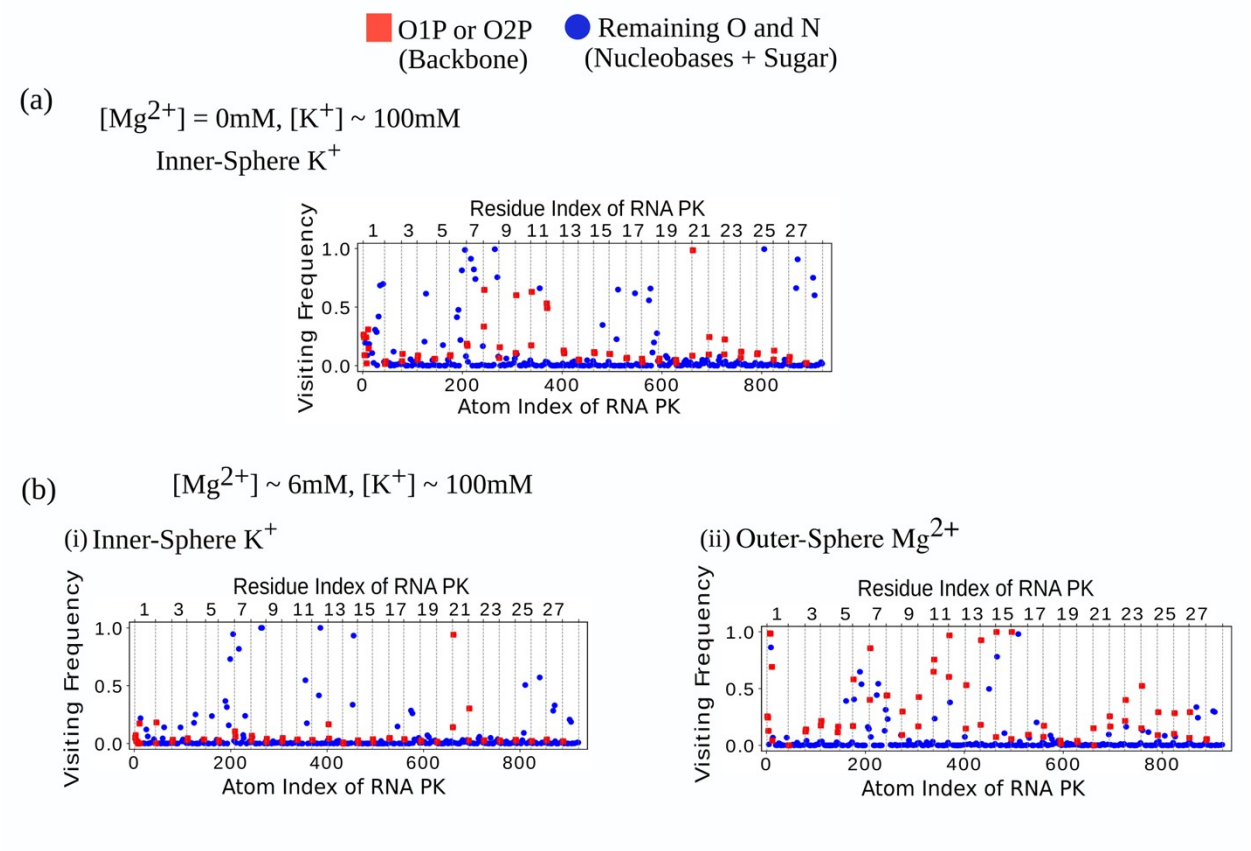

Figure S5: Preferential interaction of monovalent and divalent ions with RNA calculated using RNA site visiting frequency over 100ns of (a) Inner-Sphere K^+ ions in the absence of Mg^{2+} at [K^+] ~ 100mM, (b) (i) Inner-Sphere K^+ in presence of Mg^{2+} and (ii) Outer-Sphere Mg^{2+}, at [Mg^{2+}] ~ 6mM and [K^+] ~ 100mM, show their preferential interaction either with O_1P and O_2P atoms of backbone phosphate (red dots) and other electronegative O and N atoms (blue dots) of RNA PK.

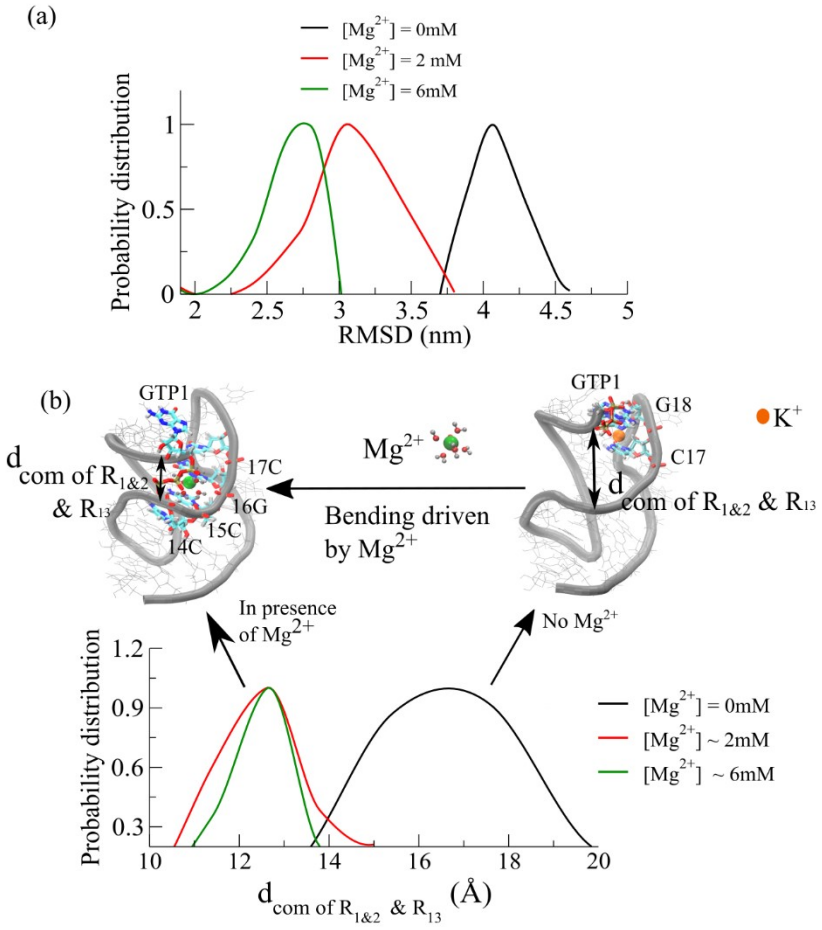

Figure S6: (a) Compaction of RNA PK and Bending of RNA PK end by outer-sphere Mg^{2+} ion. (a) Distribution of Root mean square deviation (RMSD) at different [Mg^{2+}] where [K^{+}]~100mM of last 200ns. **(b)** Distribution of distance between center of mass (com) residue 1 and 2 with 13 at different [Mg^{2+}] where [K^{+}]~100mM of last 200ns, shows bending at the 5' terminal. Representative snapshot showing minor groove narrowing after the addition of 1.6 mM Mg^{2+} to 0 mM Mg^{2+}, maintaining [K^{+}]~100 mM.

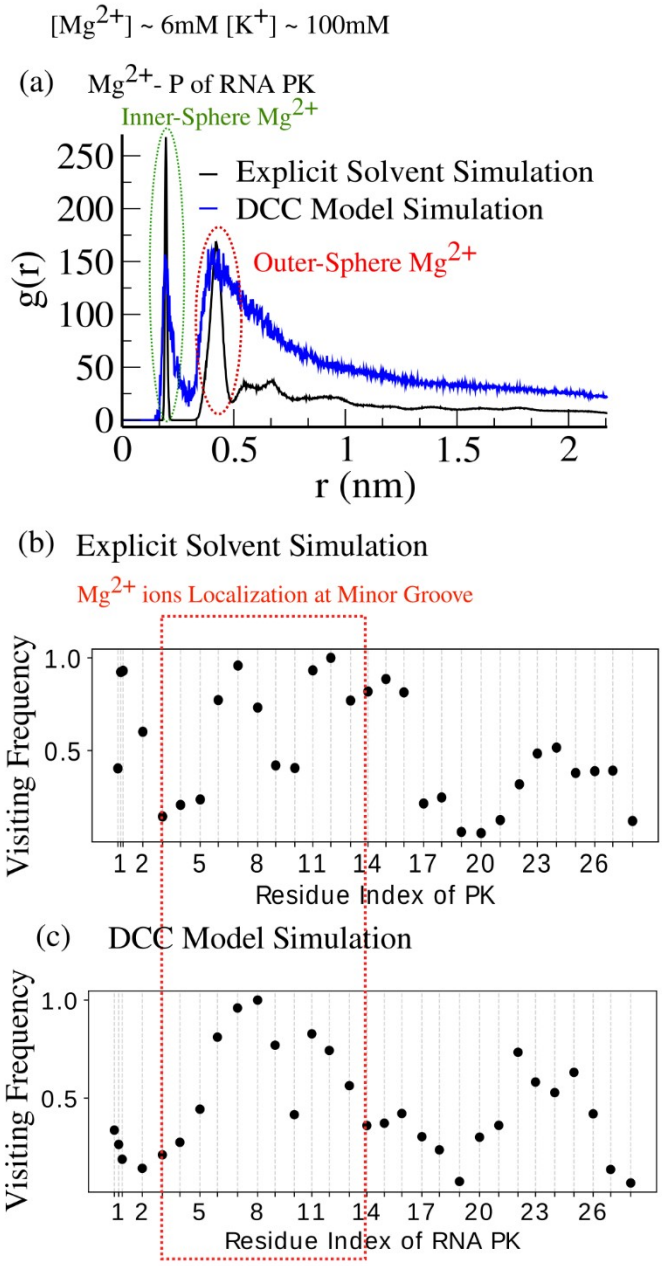

Figure S7: Detecting a spine outer-sphere Mg^{2+} ions in the minor groove region formed between Stem 1 and Stem2 from all-atom explicit solvent simulations and coarse-grained dynamic counter-ion condensation (DCC) model of RNA. (a) Comparison of RDF of Mg^{2+} ions around the Phosphate of RNA PK between Explicit Solvent simulation and DCC model simulation. Site visiting frequency showing ion-localization for outer-sphere Mg^{2+} on the phosphate groups of RNA PK measured from (b) all-atom explicit simulations of last 300ns and (c) DCC model simulation, at $[Mg^{2+}]$ ~ 6mM and $[K^{+}]$ ~ 100mM.

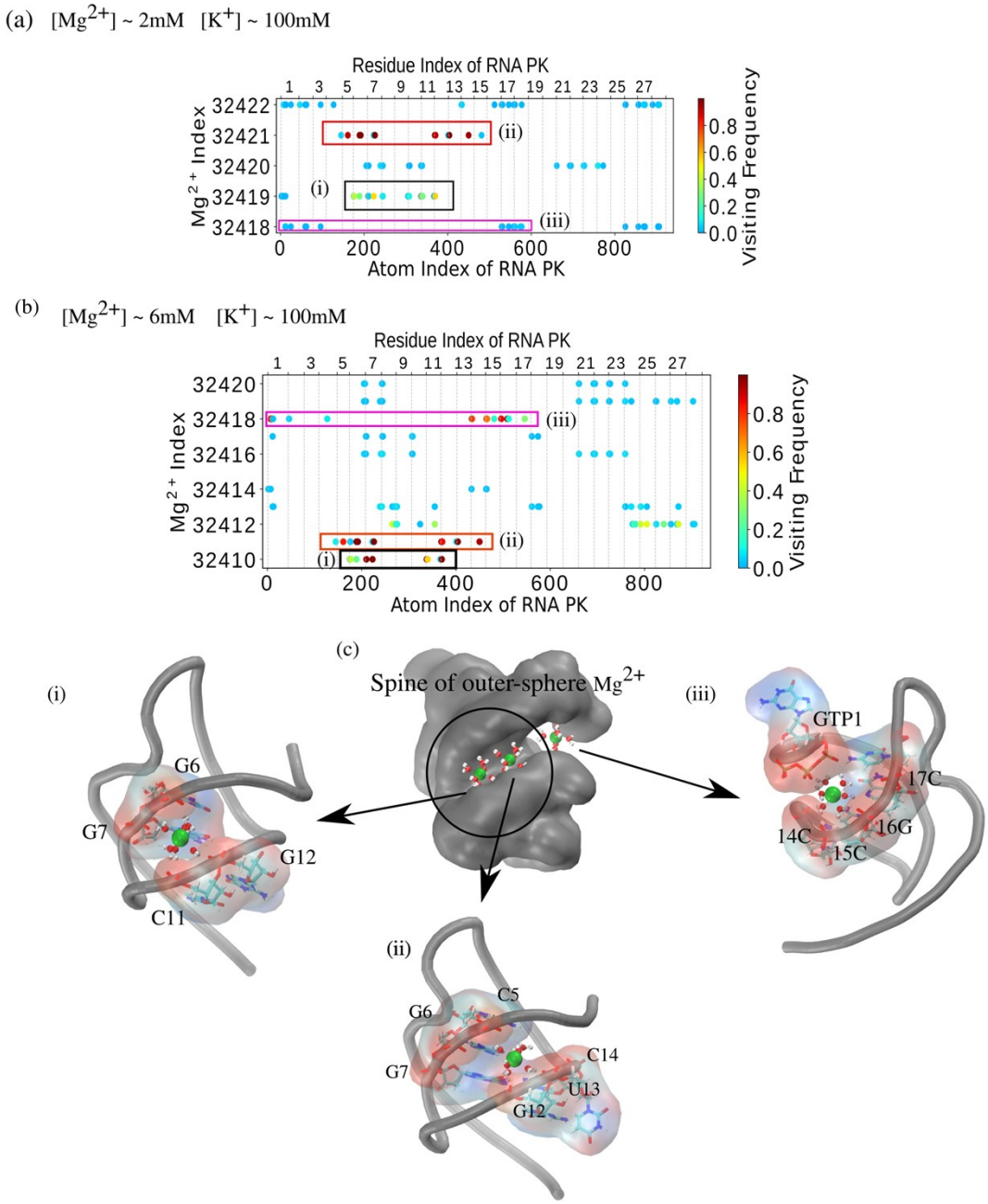

Figure S8: Contact probability map of Outer-Sphere Mg^{2+}ions and O and N of RNA PK with condition that K^+ makes contact with at least 3 atoms of RNA and minimum time should be greater than 2ns at (a) $[Mg^{2+}]$ ~ 2mM and $[K^+]$ ~ 100mM, and (b) $[Mg^{2+}]$ ~ 6mM and $[K^+]$ ~ 100mM, of 100ns demonstrate (c) Significant Outer-Sphere Mg^{2+} ions such as (i) & (ii) Spine of Mg^{2+} ions in the minor groove formed between the stem1 and stem 2 and (iii) a single outer-Sphere Mg^{2+} ion

connect GTP with 14C, 15C, 16G and 17C, all Snapshots are taken from $[Mg^{2+}] \sim 2mM$ and $[K^{+}] \sim 100mM$ simulation.

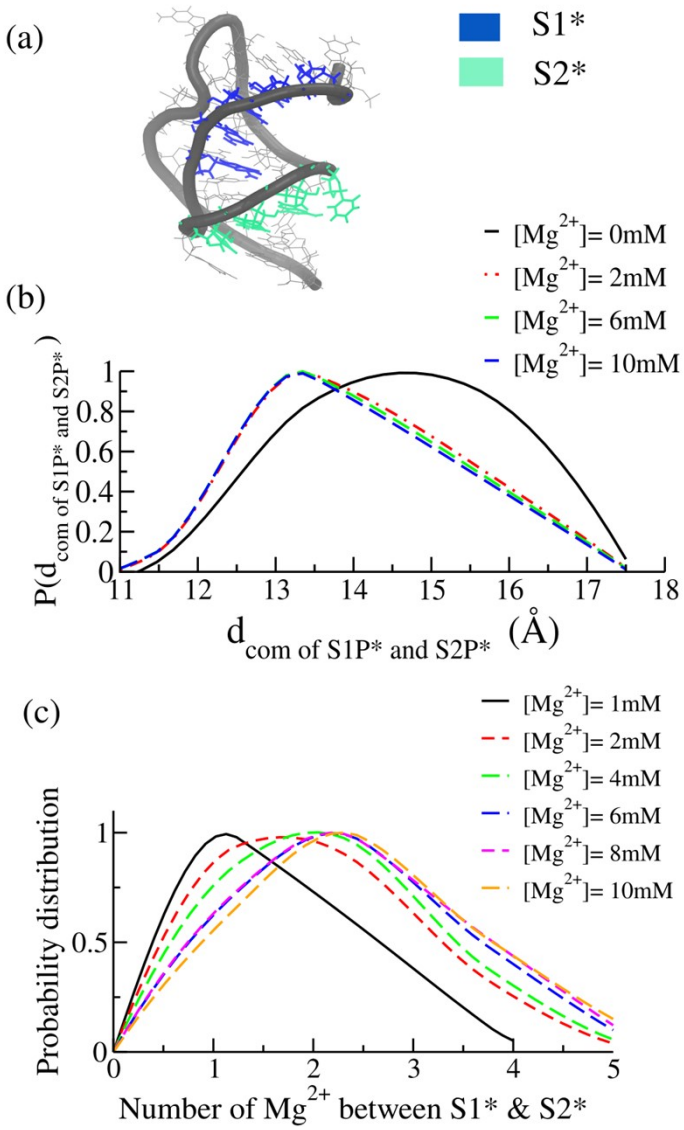

Figure S9: DCC model simulations are able to capture the localization of Mg^{2+} ions at the minor groove formed between Stem1 and Stem2, and the minor groove narrows by adding Mg^{2+} ions. (a) Image showing the minor groove formed between stem1 and stem2. (b) Distance distribution showing $[Mg^{2+}]$ dependent variation in S1P* and S2P* segment constituting a minor groove of the RNA-PK at a fixed 100mM K^{+} from DCC model simulation data. (c) Distribution of number of Mg^{2+} ions between the minor groove showing $[Mg^{2+}]$ dependent variation at a fixed 100mM K^{+} from DCC model simulation data.

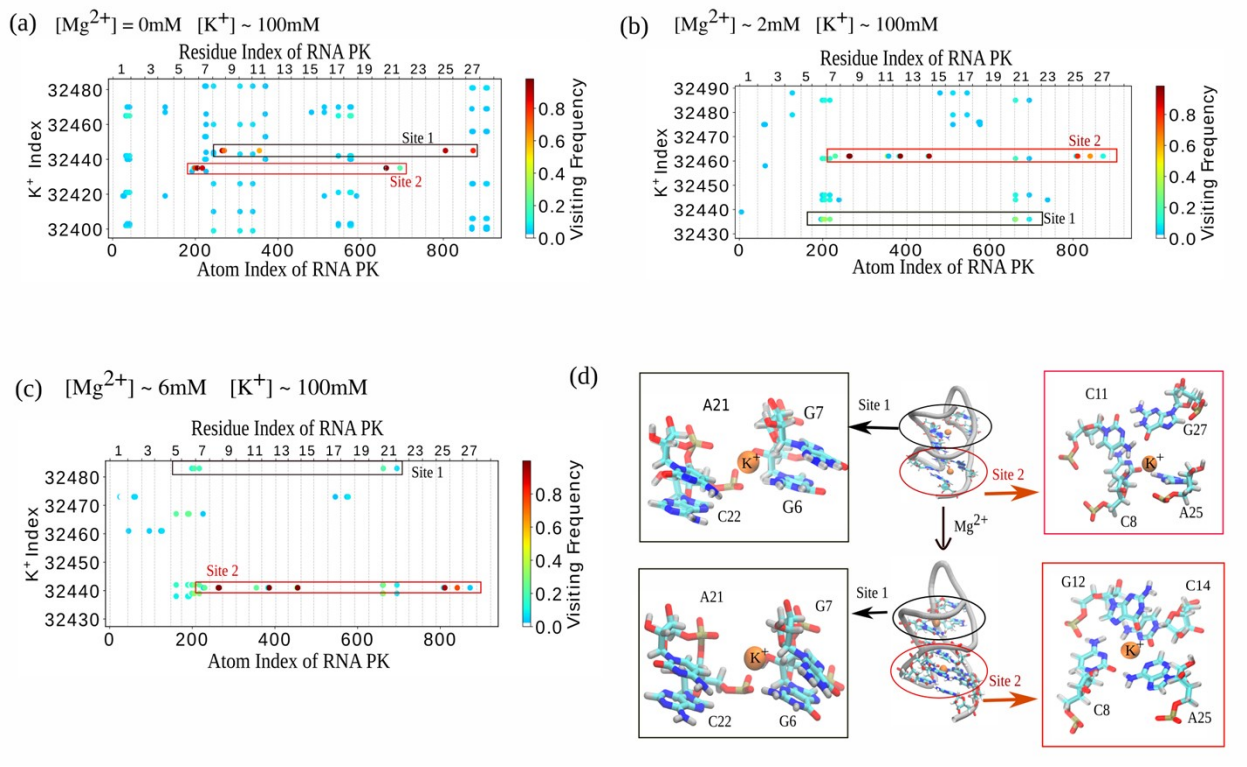

Figure S10: Contact probability map of K^+ and O and N of RNA PK over 100ns with condition that K^+ makes contact with at least 3 atoms of RNA and minimum time should be greater than 2ns are only considered at (a) $[Mg^{2+}] = 0$mM and $[K^+] \sim 100$mM, (b) $[Mg^{2+}] \sim 2$mM and $[K^+] \sim 100$mM, and (c) $[Mg^{2+}] \sim 6$mM and $[K^+] \sim 100$mM, showing (d) two active chelation stites such as site 1 and site 2 whether Upper: in absence of Mg^{2+} (Snapshot taken from $[Mg^{2+}] = 0$mM and $[K^+] \sim 100$mM) or Lower: in presence of Mg^{2+} (Snapshot taken from $[Mg^{2+}] \sim 2$mM and $[K^+] \sim 100$mM).

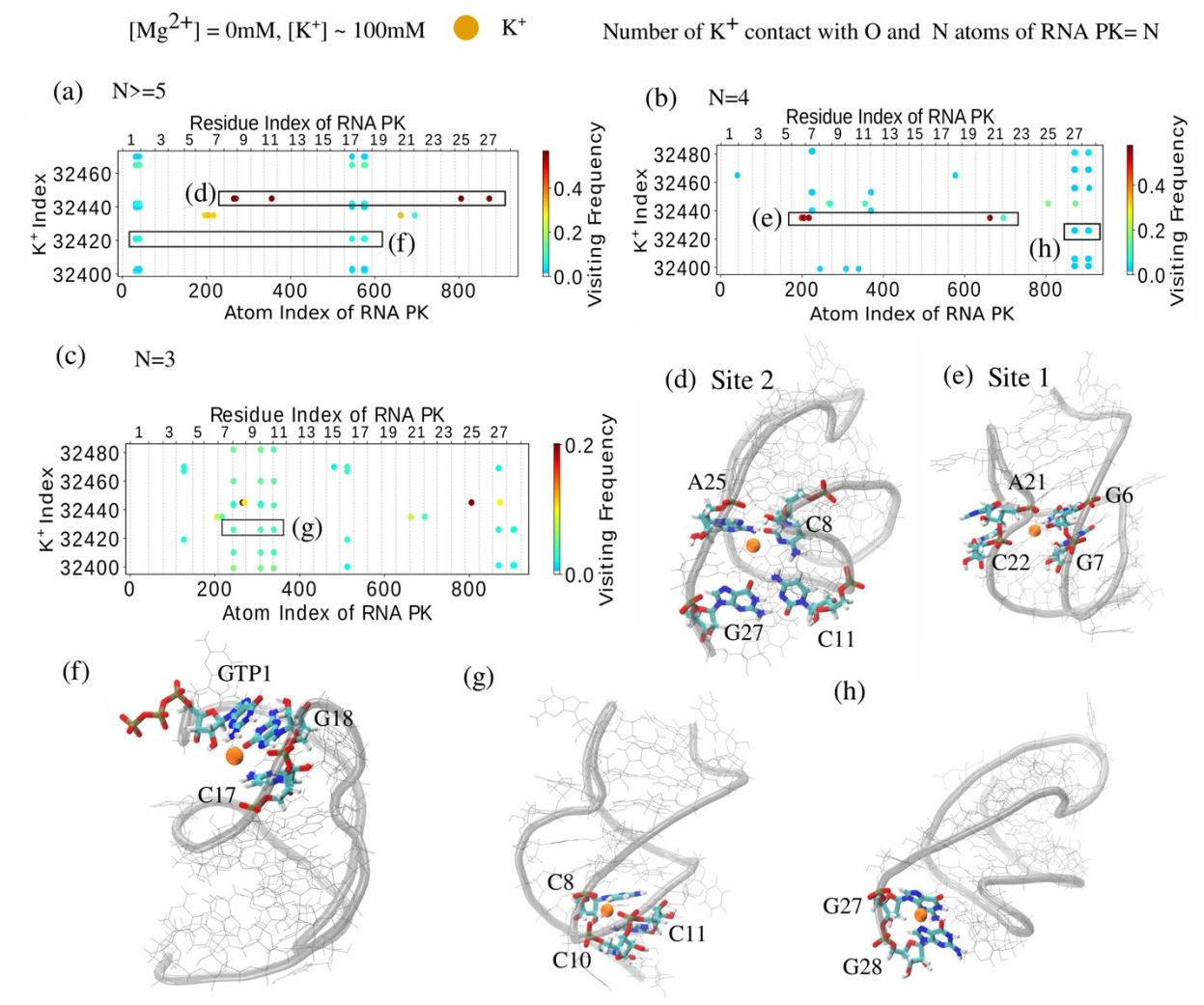

Figure S11: Using Contact probability map of inner-sphere K^+ ions and O and N of RNA PK with the condition that K^+ have minimum time to be greater than 2ns and varying number of K^+ contact with O and N atoms of RNA PK (N) from (a) N is greater than equal to 5 (b) N is equal to 4 and (c) N is 3. Five chelation sites such as (d) site2, (e) site1, (f), (g) and (h) are detected.

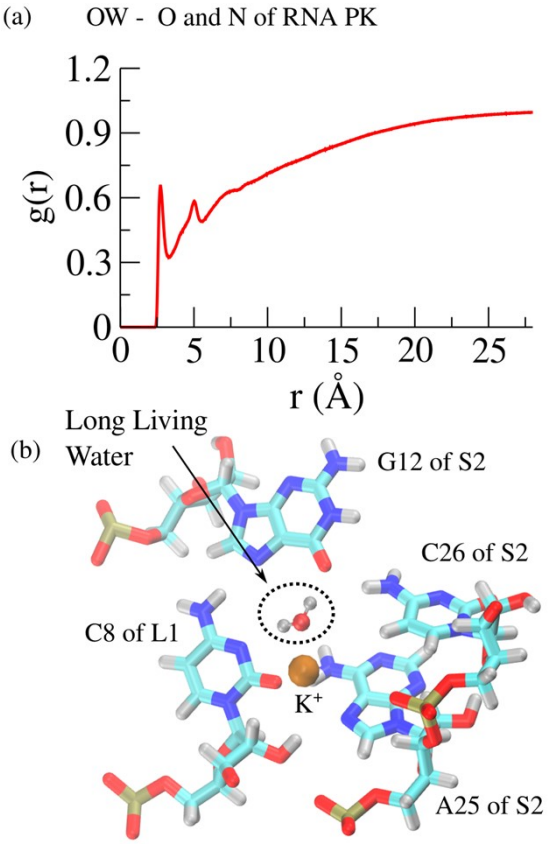

Figure S12: Water plays a significant role in stabilizing base quadruple. (a) RDF of OW around the O and N of RNA PK. (b) Image showing long living water of the first layer of K^+ ion and base quadruple, taken at $[Mg^{2+}] \sim 2mM$ and $[K^+] \sim 100mM$.

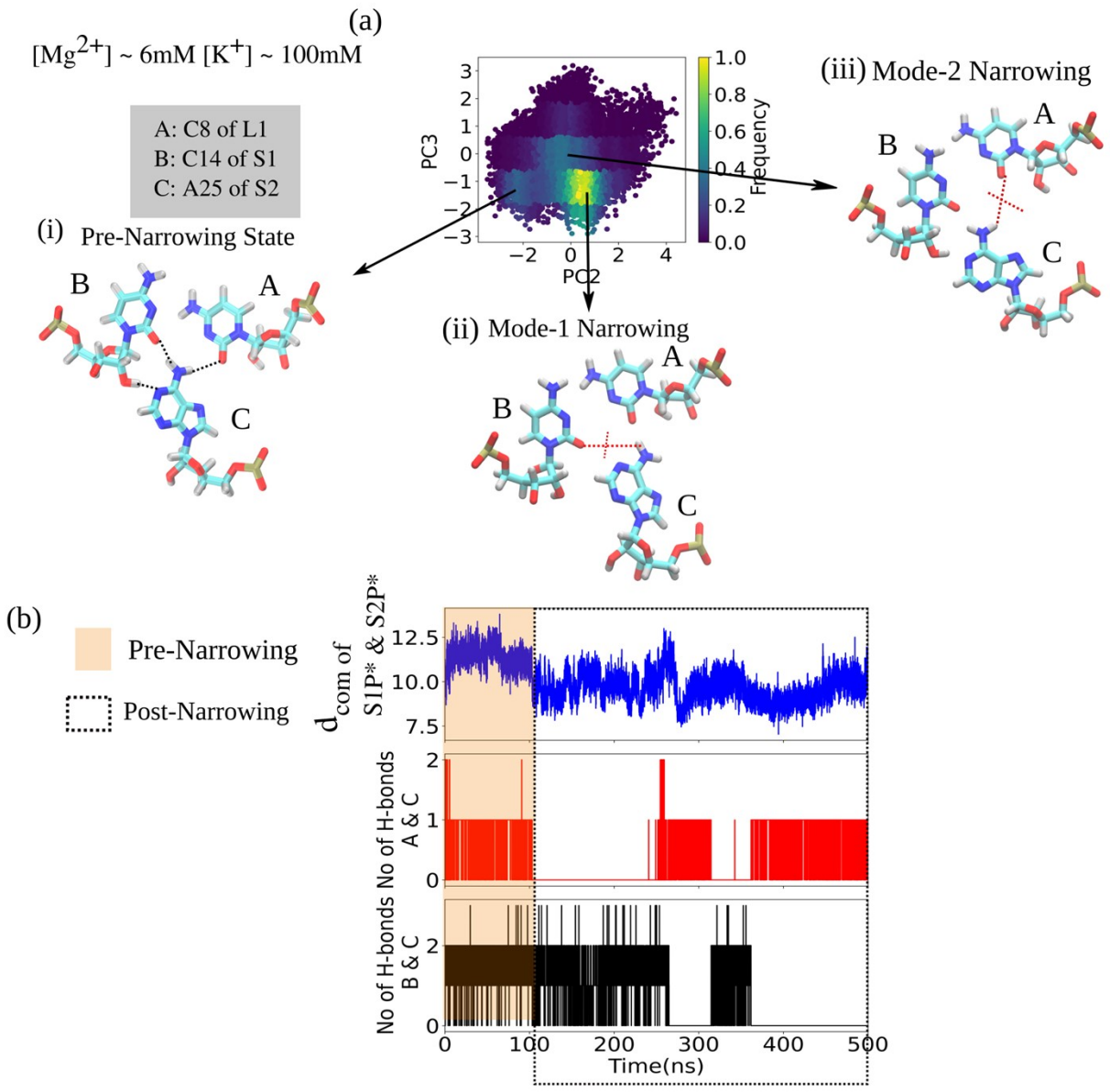

Figure S13: Distortion of the base triple with narrowing of minor groove. (a) PCA analysis of PC2 vs PC3 of 400ns of $[Mg^{2+}]$ ~ 6mM and $[K^{+}]$ ~ 100mM. Different conformation of base triple based on minor-groove breathing are (i) Pre-narrowing State, base triple is well formed, (ii) Mode-1 Narrowing, A25 of S2 move away from C14 of S1, and (iii) Mode-2 narrowing, A25 of S2 move away from C8 of L1. (b) Comparison of pre-narrowing and post-narrowing state, (i) Time-dependent evolution of distance between between com of S1* and S2* (ii) Time-dependent evolution of the number of hydrogen bonds between Residue 8 and 25 (iii) Time-dependent evolution of the number of hydrogen bonds between Residue 14 and 25, at $[Mg^{2+}]$ ~ 6mM and $[K^{+}]$~100 mM.

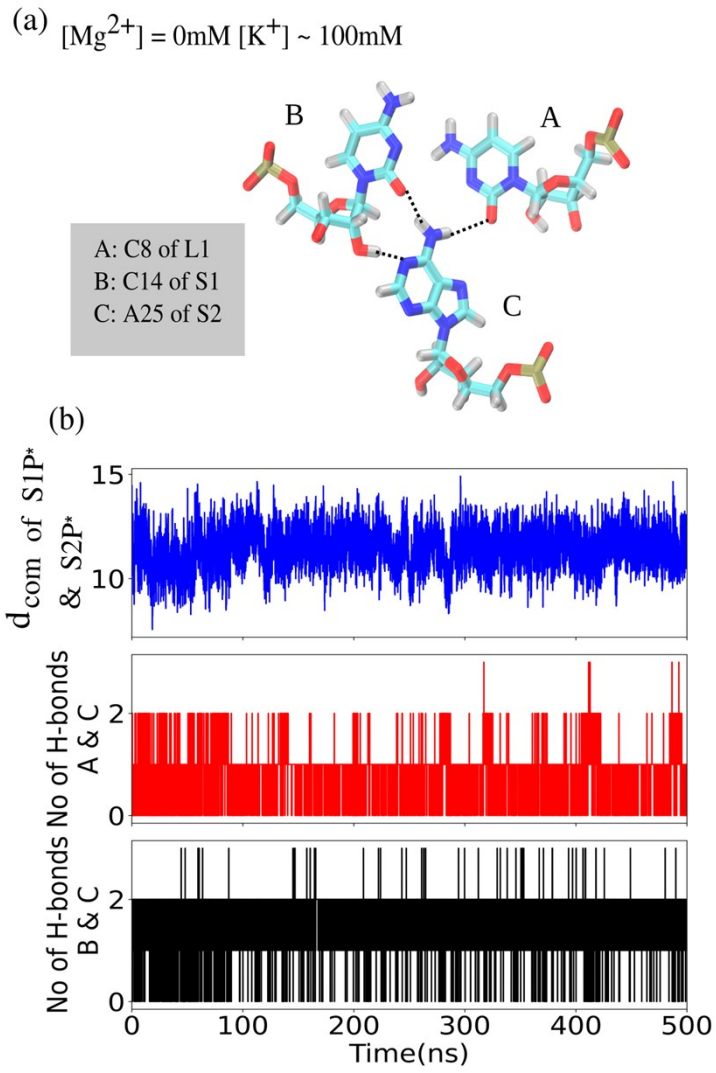

Figure S14: Base triple conformation in absence of Mg^{2+}. (a) Base triple image taken at $[Mg^{2+}]$ ~ 0mM and $[K^{+}]$~112 mM. (b) (i) Time-dependent evolution of distance between between com of S1* and S2* (ii) Time-dependent evolution of the number of hydrogen bonds between Residue 8 and 25 (iii) Time-dependent evolution of the number of hydrogen bonds between Residue 14 and 25, at $[Mg^{2+}]$ = 0mM and $[K^{+}]$ ~ 100 mM.

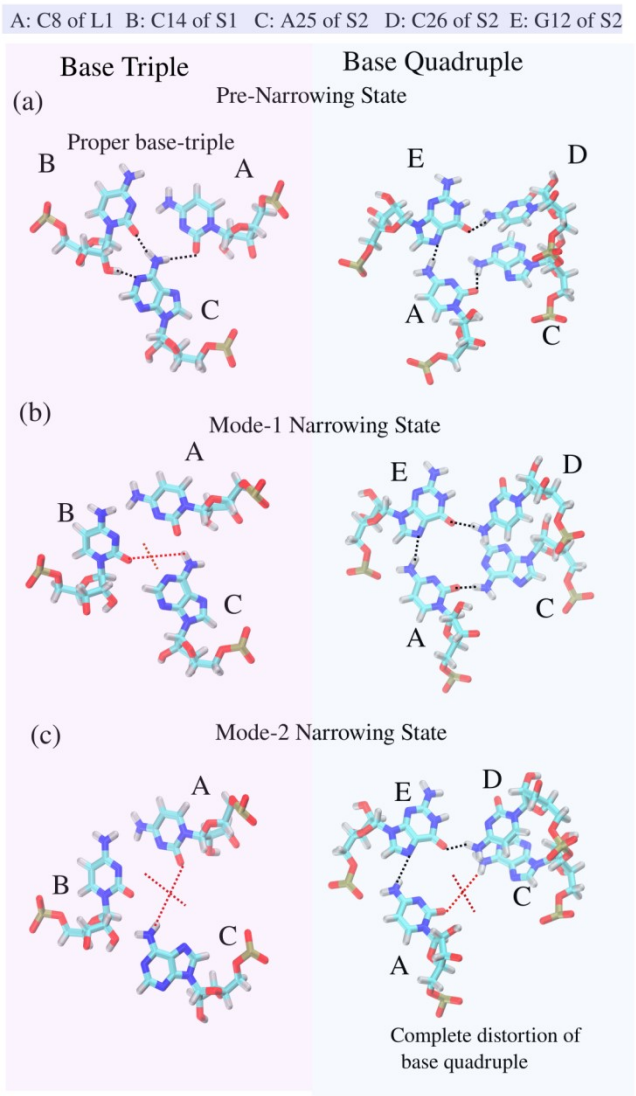

Figure S15: Different conformation of base triple and quadruple base interactions based on minor-groove breathing are (a) Pre-Narrowing state; Left: base triple is well formed. Right: Corresponding quadruple base interaction, (b) Mode-1 Narrowing; left: A25 of S2 moves away from C14 of S1 in the base triple. Right: Enlarged quadruple base interaction and (c) Mode-2 narrowing, A25 of S2 move away from C8 of L1 in the base triple. Right: completely distorted quadruple base interaction. Representative snapshot showing base triple and quadruple taken from at $[Mg^{2+}] \sim 2mM$ and $[K^{+}] \sim 100mM$.

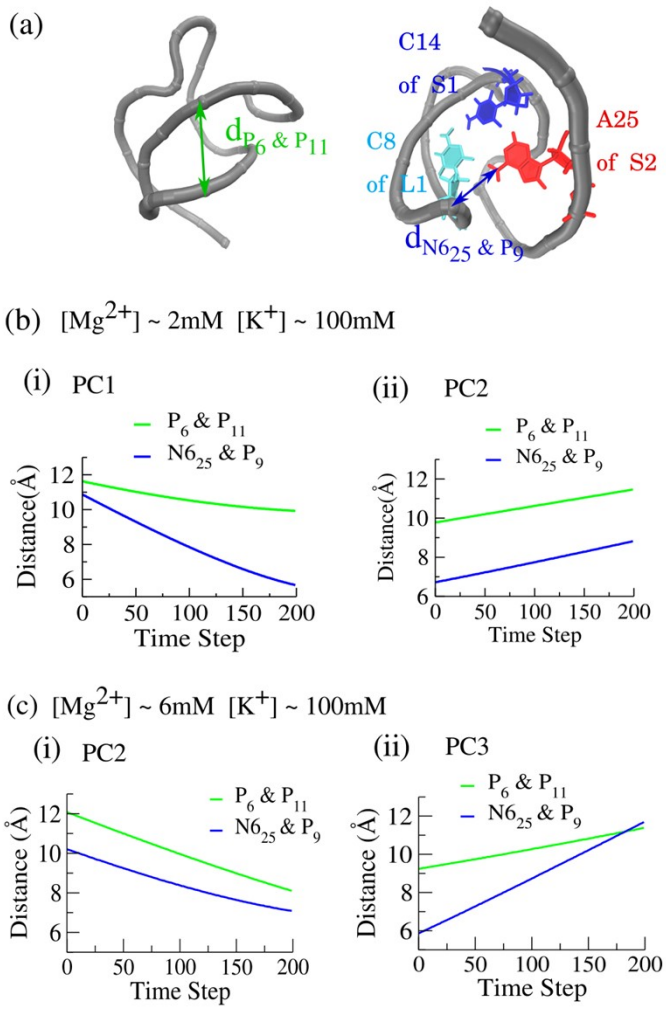

Figure S16: Correlation between Minor groove narrowing and base triple conformations are quantified using Principal component analysis. (a) Left: Image showing the minor groove distance ($d_{P6\&P11}$); Right: Image showing distance between N6 atom of residue 25 and P atom of residue 9 ($d_{N625\ \&\ P9}$) used to quantify the motion of residue 25. $d_{P6\&P11}$ and $d_{N625\ \&\ P9}$ are directly correlated in two concentrations: (b) (i) PC1 shows $d_{P6\&P11}$ and $d_{N625\ \&\ P9}$ decreases; (ii) PC1 shows $d_{P6\&P11}$ and $d_{N625\ \&\ P9}$ increases, at $[Mg^{2+}]$ ~ 2mM and $[K^+]$ ~ 100mM and (c) (i) PC2 shows $d_{P6\&P11}$ and $d_{N625\ \&\ P9}$ decreases; (ii) PC3 shows $d_{P6\&P11}$ and $d_{N625\ \&\ P9}$ increases, at $[Mg^{2+}]$ ~ 6mM and $[K^+]$ ~ 100mM.

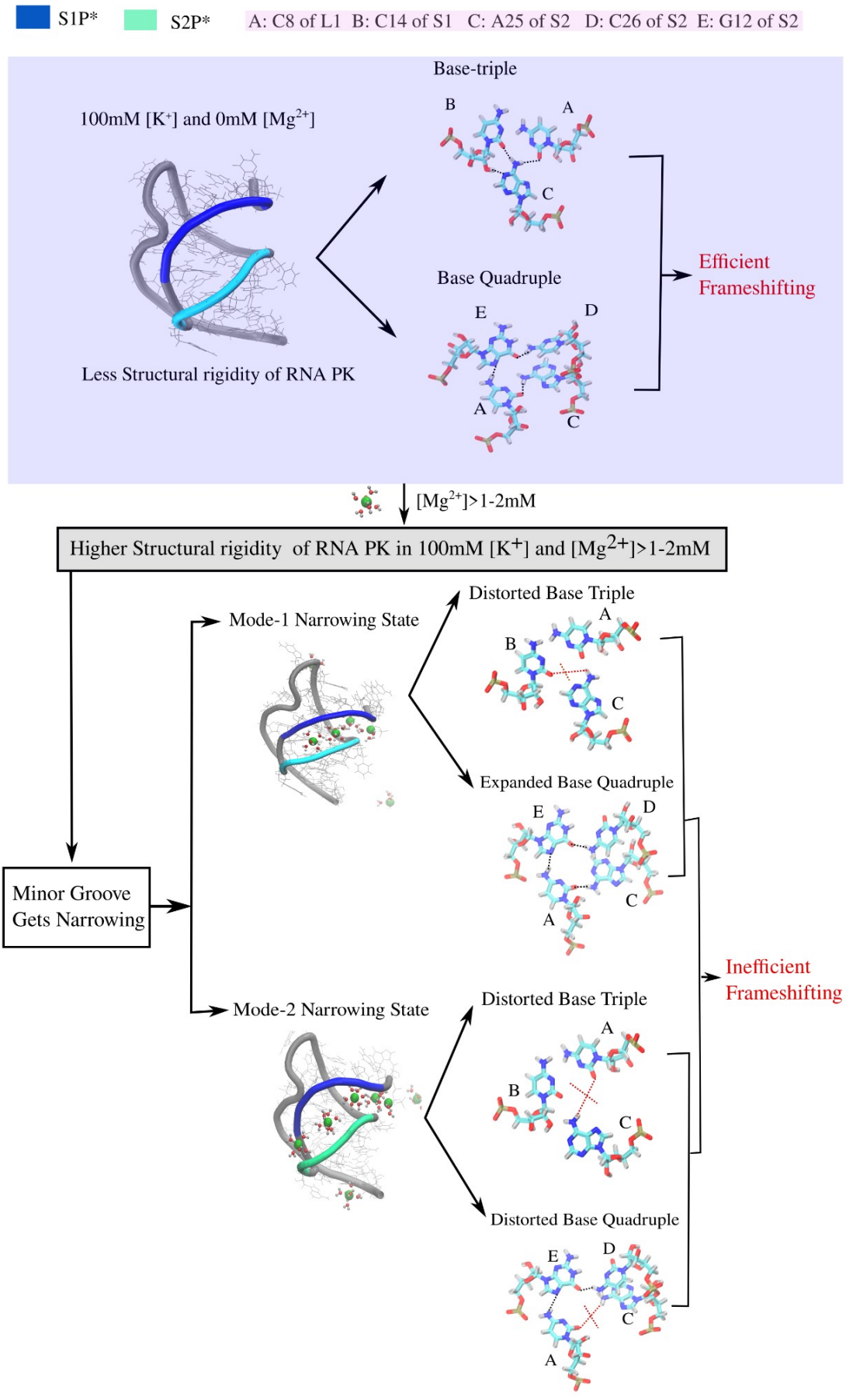
S1P*
S2P*
A: C8 of L1 B: C14 of S1 C: A25 of S2 D: C26 of S2 E: G12 of S2
Base-triple
100mM [K+] and 0mM [Mg2+]
B
A
C
Base Quadruple
E
D
A
C
Efficient Frameshifting
Less Structural rigidity of RNA PK
[Mg2+]>1-2mM
Higher Structural rigidity of RNA PK in 100mM [K+] and [Mg2+]>1-2mM
Minor Groove Gets Narrowing
Mode-1 Narrowing State
Distorted Base Triple
Expanded Base Quadruple
Mode-2 Narrowing State
Distorted Base Triple
Distorted Base Quadruple
Inefficient Frameshifting

Figure S17: Schematic illustration of structure-function connection of BWYV RNA-PK.

Experimental Mutational studies[11] on BWYV RNA PK have shown the importance of interactions of C8 of L1 with Stem2 and A25 of S1 with C14 of S1 on the ribosomal frameshifting efficiency as described in the main text.

References

1. A. Rich, L. Su, L. Chen, M. Egli and J. M. Berger, *Nature Structural Biology*, 1999, **6**, 285–292.
2. J. Wang, P. Cieplak and P. A. Kollman, *Journal of Computational Chemistry*, 2000, **21**, 1049–1074.
3. A. Pérez, I. Marchán, D. Svozil, J. Sponer, T. E. Cheatham, C. A. Laughton and M. Orozco, *Biophysical Journal*, 2007, **92**, 3817–3829.
4. M. Zgarbová, M. Otyepka, J. Šponer, A. Mládek, P. Banáš, T. E. Cheatham and P. Jurečka, *Journal of Chemical Theory and Computation*, 2011, **7**, 2886–2902.
5. R. L. Hayes, J. K. Noel, A. Mandic, P. C. Whitford, K. Y. Sanbonmatsu, U. Mohanty and J. N. Onuchic, *Physical Review Letters*, 2015, **114**.
6. M. Egli, G. Minasov, L. Su and A. Rich, *Proceedings of the National Academy of Sciences*, 2002, **99**, 4302–4307.
7. L. X. Dang, *Journal of the American Chemical Society*, 1995, **117**, 6954–6960.
8. O. Allnér, L. Nilsson and A. Villa, *Journal of Chemical Theory and Computation*, 2012, **8**, 1493–1502.
9. M. T. Panteva, G. M. Giambaşu and D. M. York, *J Comput Chem*, 2015, **36**, 970–982.
10. K. K. Grotz and N. Schwierz, *J Chem Phys*, 2022, **156**, 114501.
11. Y.-G. Kim, L. Su, S. Maas, A. O'Neill and A. Rich, *Proceedings of the National Academy of Sciences*, 1999, **96**, 14234–14239.